Nano World Journal

https://doi.org/10.17756/nwj.2022-s1-014

Research Article

Open Access

Influence of Nitrate on the Growth of Calcium Hydroxide Nanoparticles

Akash[1], Harish[1], Virendra Singh Chouhan[2*], Rahul Singhal[3], Anoop Kumar Mukhopadhyay[4], and Pushpendra Kumar[1*]

[1]*Department of Physics, Manipal University Jaipur, Rajasthan, India*

[2]*Department of Mathematics and Statistics, Manipal University Jaipur, Rajasthan, India*

[3]*Department of Physics, Malaviya National Institute of Technology Jaipur, Rajasthan, India*

[4]*Department of Physics, Sharda School of Basic Sciences and Research, Sharda University, Greater Noida, Uttar Pradesh, India*

***Correspondence to:**
Virendra Singh Chouhan
Department of Mathematics and Statistics, Manipal University Jaipur, Rajasthan, India
E-mail: darbarvsingh@yahoo.com

Pushpendra Kumar
Department of Physics, Manipal University Jaipur, Rajasthan, India
E-mail: pushpendra.kumar@jaipur.manipal.edu

Received: August 23, 2022
Accepted: October 17, 2022
Published: October 20, 2022

Citation: Akash, Harish, Chouhan VS, Singhal R, Mukhopadhyay AK, et al. 2022 Influence of Nitrate on the Growth of Calcium Hydroxide Nanoparticles. *NanoWorld J* 8(S1): S69-S75.

Published by United Scientific Group

Abstract

In the present work, we have synthesized the calcium hydroxide ($Ca(OH)_2$) nanoparticles (NPs) with different molarity of calcium nitrate tetrahydrate. The $Ca(OH)_2$ NPs were synthesized by a simple chemical route. The molarity of calcium nitrate tetrahydrate was varied in the range of 0.4, 1, and 1.6 M by keeping the molarity of sodium hydroxide (NaOH) constant. All the procedure was done at room temperature. The prepared three samples were characterized using X-ray diffraction (XRD), field emission scanning electron microscope (FESEM), Fourier transform infrared spectroscopy (FTIR) and Ultraviolet-Visible (UV-Vis) spectroscopy techniques. From the XRD spectra results, it was seen that in comparison to $Ca(OH)_2$ prepared at 0.4 M, the crystallite size of $Ca(OH)_2$ prepared at 1.6 M decreased drastically.

Keywords

Calcium nitrate tetrahydrate, Calcium hydroxide, Molarity variation

Introduction

$Ca(OH)_2$ (slaked lime) has various applications in the industries, paper production, energy storage, and endodontics treatment owed to its non-toxicity and low cost [1-6]. The reversible reaction of $Ca(OH)_2$ [$Ca(OH)_2 \leftrightarrow CaO + H_2O$] has been investigated for energy storage applications and discovered that the anticipated equilibrium temperature at 1 bar H_2O partial pressure is 505 °C and the reaction enthalpy is 104.4 kJ/mol [1]. The reversible reaction of ($Ca(OH)_2$) to (CaO) and water vapour is also used in the circumstance of energy storage. The operation of the system at the low pressure enhances the integration possibilities and also increases the overall storing efficiency of the thermochemical system [2]. Due to its high energy density and ability of durable storage, $Ca(OH)_2$ has attracted considerable attention of other researchers [3, 4]. It is also used in various industries alternating from food to green remediation. The $Ca(OH)_2$ formed in low temperature process with a specific CO_2 intensity can uptake more CO_2 compared to its related material with its specific production forming a basis for a truly CO_2-negative material [5]. The study of commercial Kraft pulps was studied by Dolle et al. and noted that the replacement of NaOH with $Ca(OH)_2$ in the oxygen bleaching phase reached finest bleaching efficiency for yellow pine Kraft pulps at 2% to 3% $Ca(OH)_2$ concentration [6]. $Ca(OH)_2$ is included in several materials and antimicrobial formulations can be used in many treatment modalities with intracanal medicaments, pulp-capping agents, and root canal sealers. $Ca(OH)_2$ paste has high pH 12.4 - 12.8 chemically classified as a

strong base. The main action of $Ca(OH)_2$ comes from calcium ions (Ca^{2+}) and hydroxyl ions (OH^-) ionic dissociation. The lethal effects of $Ca(OH)_2$ on bacterial cells are probably due to protein denaturation and damage to DNA and cytoplasmic membranes [7]. $Ca(OH)_2$ prepared by simple precipitation method shows photocatalysts activities on against methylene blue (MB). The process was held under Visible light radiation. Through indirect dye photosensitization it was found that MB was photocatalytically degraded over $Ca(OH)_2$ [8]. In an aqueous solution, $Ca(OH)_2$ separates into Ca^{2+} ions and OH^- ions. The highly alkaline nature of this material comes from the OH^- ions, which is bactericidal in nature. Whereas, in the remineralization process Ca^{2+} ion plays an important role [9]. Researchers found that employing calcium oxides created by calcining limestone, CaO, and $Ca(OH)_2$ as solid base catalysts for the transesterification of soybean oil and ethanol led to the catalytic activities were strongly influenced by the base site strengths and the structures of the catalysts. By adding $Ca(OH)_2$ to CaO and calcining it at a high temperature, CaO's catalytic activity can be improved [10]. Despite of having an extensive range of uses of $Ca(OH)_2$ NPs, there are only a few reports that present the effect of molarity on the applications of $Ca(OH)_2$ NPs. Hence, this lack of knowledge makes the scope of the current study. In this paper, the effect of nitrate molarity on the structural and optical properties of $Ca(OH)_2$ NPs was studied. The synthesized material was characterized using several techniques that includes XRD, FTIR, FESEM, and UV-Vis spectroscopy.

Materials and Methods

The $Ca(OH)_2$ nanoparticles were synthesized by the simple chemical precipitation route. In this process, the calcium nitrate tetrahydrate ($Ca(NO_3)_2.4H_2O$) and sodium hydroxide (NaOH) from Merck, Bengaluru were used without any further purification. The $Ca(OH)_2$ was made in an aqueous solution at normal temperature using a simple precipitation method. In the present work, we have synthesized three $Ca(OH)_2$ samples with different concentrations of nitrate. First, 1 M NaOH and 0.4 M $Ca(NO_3)_2.4H_2O$ solutions were prepared in distilled water. The precipitator NaOH solution was mixed dropwise with the rate of 3 ml/min in the precursor of $Ca(NO_3)_2.4H_2O$ solution. The entire process was conducted at room temperature while continuous mixing on magnetic stirrer at 1200 rpm. After half an hour of the process, the white precipitate was formed. The obtained white precipitate was filtered using Whatman filter paper. The obtained white powder of $Ca(OH)_2$ was not washed deliberately to keep the nitrate content in the synthesized samples. The following is a description of the chemical reaction for $Ca(OH)_2$ nanoparticles synthesis at room temperature:

$$Ca(NO_3)_2.4H_2O + 2NaOH \rightarrow Ca(OH)_2 + 2NaNO_3 + 4H_2O \quad (1)$$

The prepared precipitate was heated in the air at 60 °C for 2 hours. Consequently, by changing the molarity of the $Ca(NO_3)_2.4H_2O$ solution from 0.4 M to 1.6 M with a gap of 0.6 M, the three powder samples were prepared using a similar process as mentioned above. The molarity of NaOH was fixed at 1 M in all the three prepared samples. The powder samples made with three different concentrations of $Ca(NO_3)_2.4H_2O$ (0.4 M, 1 M, and 1.6 M) solution are hereafter named respectively as C1, C2, and C3. All the prepared samples were then characterized by various techniques such as XRD, FESEM, FTIR, and UV-Vis spectroscopy. The results of some characterization techniques are mentioned in the Table1.

Structural analysis

The XRD was used to investigate the crystallinity of all the prepared samples. For this purpose, a Rigaku Miniflex-II X-ray diffractometer was used with the Cu K_α monochromatic radiation (λ = 1.506 Å). The XRD data was recorded using an angular range (2θ) of e.g., $15° \leq 2\theta \leq 80°$ at normal temperature with a scanning step of 0.02°.

Microstructural analysis

All powder samples were examined for morphology and microstructure using a standard (JEOL JSM-7610FPlus, Japan). To determine the elemental makeup of the samples as they were created, an energy dispersive X-ray (EDX) spectrometer coupled to the FESEM was used.

Optical analysis

The optical study was carried out with UV-Vis spectroscopy analysis. A UV-Vis spectrophotometer (Shimadzu UV-NIR 2600, Japan) was used for this purpose. To get uniform dispersion, all the prepared samples were dissolved in ethanol and ultrasonicated for half an hour. The UV-Vis spectrum was recorded with a wavelength range of 190 - 800 nm. The Tauc's plots were plotted to calculate the energy band gap using the obtained absorbance spectrum of all the samples.

Surface functional analysis

An FTIR spectrometer (Bruker Alpha, USA) was used on dry samples for the analysis of infrared absorption. The data were acquired between the spectral range of 500 to 4000 cm^{-1}.

Results and Discussion

XRD study

The XRD spectrum of all the prepared samples noted using an X-ray diffractometer that is mentioned in Figure 1. The several peaks were observed in the XRD spectrum shown in Figure 1. The different peaks at 2θ values for all the samples are 18.24°, 28.83°, 34.32°, 47.29°, 51.03°, 54.48°, 62.81°, 64.48°, and 71.96° correlated respectively to the following planes (001), (100), (101), (102), (110), (111), (201), (112), and (202) assigned in the XRD spectrum. The detected diffraction peaks match with the $Ca(OH)_2$ phase as the main phase with space group p- 3 m1 (Space Group No: 164, PDF Card No. 00–004-0733) [11]. The $NaNO_3$ salt was also found in the $Ca(OH)_2$ samples, confirmed by the XRD analysis [12]. The peaks related to nitrate are marked in the Figure 1 by star and confirm the presence of nitrate in the synthesized samples. The $NaNO_3$ has a high solubility in the water. The $NaNO_3$

formed due to the ion exchange process in an aqueous solution and it comes as a residual impurity in the filtered powdery precipitates of $Ca(OH)_2$ [12]. The crystallite size and lattice strain were calculated using by the well-known Williamson-Hall technique which is given below [13]:

$$\beta \cos\theta = \frac{k\lambda}{t_{W-H}} + 4\varepsilon \sin\theta \qquad (2)$$

Where β is the full width half maxima, k is a constant; and θ is the diffraction angle. All the measured data were fitted to compute the lattice strain and the crystallite size. The lattice strain values were obtained from the slope and crystallite size was calculated by y-intercepts of the trend lines obtained after fitting the measured data points. The W-H plots for samples C1, C2, and C3 are respectively shown in Figure 2a, 2b and 2c. The value of crystallite size and the lattice strain of all the samples are shown in Table 1. For the samples C1, C2, and C3 the crystallite size was estimated respectively to be 103.47 nm, 65.40 nm, and 64.49 nm. The crystallite size of sample C3 decreased by nearly 38% compared to the crystallite size of sample C1. The lattice strain of the sample C1 was considered to be ~ 1.485×10^{-3}. Further, the lattice strain of samples C2 and C3 were decreasing to ~ 0.94×10^{-3} and ~ 0.72×10^{-3}, respectively. The positive slope of the trend line indicates that the lattice strain is tensile for all the samples as shown in Figure 2. The tensile strain was decreasing as the molarity of $Ca(NO_3)_2.4H_2O$ was increasing in samples C2 and C3 compared to sample C1. The value of crystallite size was highly influenced by lattice strain, as shown by Equation (2). Because lattice strain drops with declining crystallite size, this decrease in strain was consistent with the smaller crystallite size [14]. The presence of $NaNO_3$ which was formed during the synthesis process mentioned in Figure 1, can also affect the crystallite size and strain of the samples. The increasing $Ca(NO_3)_2.4H_2O$ concentration results in an increase in the amount of $NaNO_3$ in all the samples Figure 3. The decrease in the crystallite size with increasing the nitrate amount was studied by other researchers also [15]. The relation between crystallite size (t_{W-H}) and dislocation density (ρ_d) is given by the below equation [16];

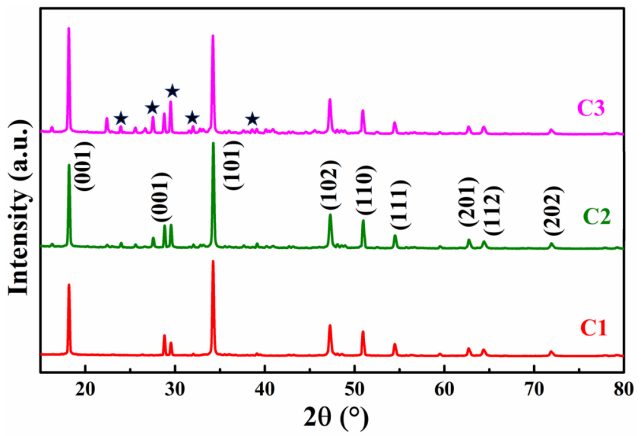

Figure 1: X-ray diffraction of the samples C1, C2, and C3.

$$P_d = \frac{1}{t_{WH}^{\ 2}} \qquad (3)$$

Higher dislocations in a given region can be accommodated by the lower crystallite size. As a result, the dislocation density (d) increases as the crystallite size decreases, and the values were listed in Table 1. In other words, the number of dislocations was estimated to be ~ 0.9×10^{14} (m^{-2}) in sample C1. However, in the case of the higher concentration sample C3; it jumps by almost an order of magnitude to ~ 2.4×10^{14} (m^{-2}). The d-spacing can be calculated for different diffraction planes using the common diffraction condition [17].

$$2d\sin\theta = n\lambda \qquad (4)$$

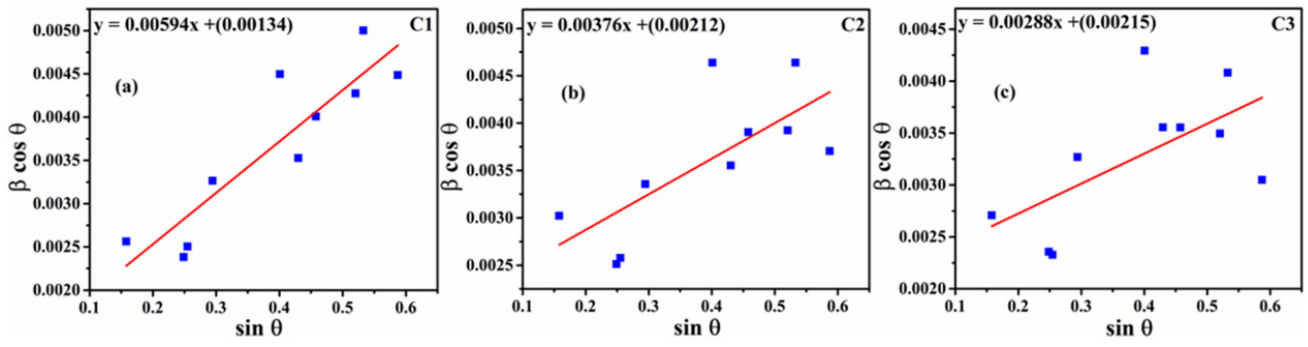

Figure 2: W-H plots of the samples (a) C1, (b) C2, and (c) C3.

Table 1: The crystallite size, band gap, strain, and dislocation density of the samples C1, C2, and C3.

Sample	Bandgap (eV)	Strain (ε)	Crystallite size, t_{W-H} (nm)	Dislocation density, δ(m^{-2})
C1	5.50	1.48×10^{-3}	103.47	$0.9 * 10^{14}$
C2	5.55	0.94×10^{-3}	65.40	$2.3* 10^{14}$
C3	5.68	0.72×10^{-3}	64.49	$2.4* 10^{14}$

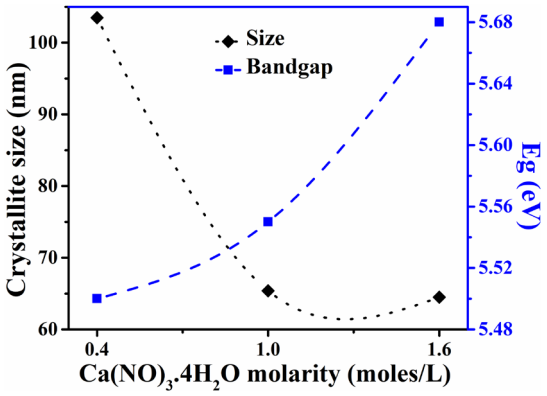

Figure 3: Crystallite size and band gap variation of the samples C1, C2, and C3.

The values of lattice parameters 'a' and 'c' are calculated by the following relation as given below [17].

$$\frac{1}{d_{hkl}^{\ 2}} = \left[\frac{4}{3}\left(\frac{h^2+k^2+hk}{a_2}\right)+\frac{l^{\ 2}}{c^2}\right] \quad (5)$$

In the above equation h, k, and l are Miller indices and d_{hkl} is the inter-planar spacing. Table 2 displays the derived values for the "a" and "c." The following equation was used to calculate the bond length (L) and unit cell volume. [18].

$$L = \sqrt{\frac{a^2}{3}+\left(\frac{1}{2}-\mu\right)^2 c^2} \quad (6)$$

$$\mu = \frac{-}{3}\left(\frac{a}{c}\right) + 0.25 \quad (7)$$

$$V = \frac{\sqrt{3}}{2}(ca^2) = 0.866(ca^2) \quad (8)$$

Table 2 displays the calculated values for the lattice parameters "a" and "c." The lattice parameter 'a' respectively for samples C1, C2, and C3 are 3.5740 Å, 3.5717 Å, and 3.5774 Å and similarly, the lattice parameter 'c' for samples C1, C2, and C3 are 4.8734 Å, 4.8702 Å, and 4.8791 Å. The 'c/a' ratio for the samples C1, C2, and C3 are 1.36357, 1.36355, and 1.36386, respectively. The unit cell volume for all the prepared samples was also calculated and mentioned in Table 2. The anion-cation bond length of samples C1, C2, and C3 were 2.2477 Å, 2.2447 Å, and 2.2523 Å correspondingly. The atomic displacement of the samples C1, C2, and C3 were 0.42928, 0.42928, and 0.42920, respectively. The measured atomic displacement and anions-cations bond length for each sample was tabulated in Table 2. Further, based on the values of a and c, the unit cell volumes of all the three samples C1, C2, and C3 were estimated and tabulated in Table 2.

FESEM study

The microstructural study of all the prepared samples was carried out by FESEM spectroscopy and all the photomicrograph of the prepared samples were shown in Figure 4. From Figure 4, it can be seen that particle size usually ranges from 50 to 400 nm. The cluster size was large compared to the particle size obtained by XRD data. This was because of the agglomeration of nanoparticles due to surface charge on nanoparticles surface through the Van der Waal interaction. It can be clearly seen that the particle size of sample C1 (Figure 4a) was more than the particle size of both samples C2 and C3 (Figure 4b and 4c). The particle size was decreasing with increasing the molarity of nitrate which was well collaborated with XRD data. Though, the molarity of nitrate was increasing in samples C2 and C3 so the $NaNO_3$ amount was also increasing in these samples. The sample C3 has the highest molarity of nitrate i.e., highest value of $NaNO_3$ present in it. Increasing the amount of nitrate typically changes the crystallite size of materials which was also discussed in the XRD portion.

FTIR spectroscopy analysis

In Figure 5 we show the FTIR spectra of all the samples C1, C2, and C3. An absorption band at ~ 3640 cm^{-1} corresponding to -OH group stretching mode can be seen in all of the spectra [19]. It further shows that all the samples have the hexagonal shape of $Ca(OH)_2$. The minor peak at ~ 2330 cm^{-1} occurs due to the CO_2 absorption stretching on the powder sample [19, 20]. The minor absorption peak at ~ 1695 cm^{-1} occurs because of atmospheric C=O stretching caused in the samples C1, C2, and C3. While the minor peak at ~ 1470 to 1510 cm^{-1} is connected to the surface absorbed CO_3 group's v3 asymmetric stretching. The surface-adsorbed CO_3

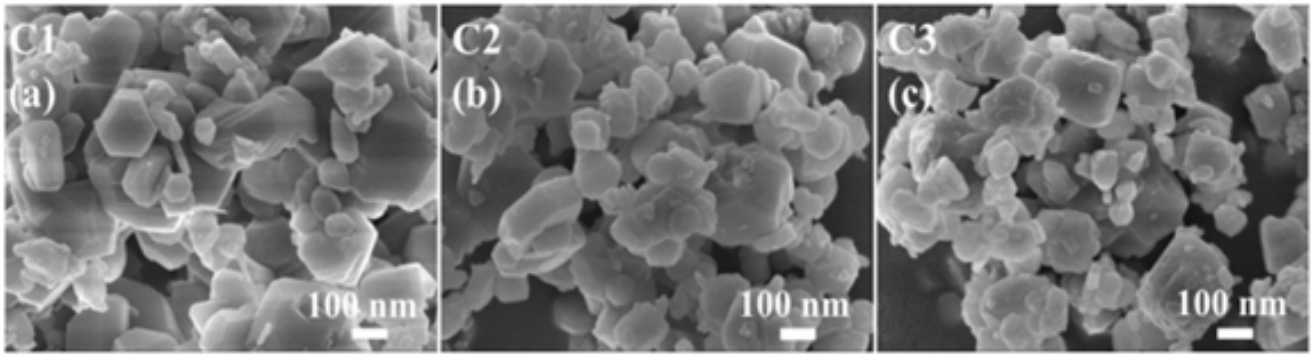

Figure 4: FESEM images of sample (a) C1, (b) C2, and (c) C3.

Table 2: Lattice parameter, atomic displacement, and bond length of the samples C1, C2, and C3.

Sample	Lattice parameters		c/a	Atomic displacement (u)	Anion-cation bond length (Å)	Volume (Å^3)
	a (Å)	c (Å)				
C1	3.5740	4.8734	1.36357	0.42928	2.24771	46.6876
C2	3.5717	4.8702	1.36355	0.42928	2.24479	46.5970
C3	3.5774	4.8791	1.36386	0.42920	2.25230	46.8312

group undergoes a v2 symmetric deformation, which results in the band at 830 cm^{-1} to 890 cm^{-1}. The current study match well with the literature reports [20]. The strongest absorption peak present at 1385 cm^{-1} is linked with asymmetric NO_3 stretch which approves the occurrence of nitrate [12]. Sample C1 shows the minor absorption peak of NO_3 stretch while in sample C3 the intensity of NO_3 stretch is much higher compared to both samples C2 and C1. The nitrate stretching peak is increasing with the increase in molarity of nitrate that can be seen in Figure 5. As anticipated, the FTIR spectra of each sample showed the band characteristics of the $Ca(OH)_2$ and $CaCO_3$ groups.

UV-Vis spectroscopy

The UV-Vis spectrophotometer analysis results for synthesized $Ca(OH)_2$ NPs at different nitrate concentration is shown in Figure 6. A gradual increase in optical absorbance was found for larger concentrations of nitrate as shown in Figure 6 in the wavelength range of (190 - 800 nm). The corresponding Tauc's plot were shown in Figure 7. A blue shift in absorbance band edge was also presented which can be due to increase in molarity of nitrate. The following equation can be used for determining the optical band gap of all the samples [13].

$$\alpha h\upsilon = A(h\upsilon - Eg)^{\frac{1}{2}} \quad (9)$$

Where 'α' is the absorption coefficient and 'A' is a constant. The obtained band gap values of the samples with different nitrate concentrations are presented in Table 1. It was observed that the band gap of all the prepared samples were increasing gradually. The band gap values were increasing from 5.50 eV to 5.68 eV with increase in the molarity of nitrate. The calculated crystallite size using W-H plot, was decreased by 38% in Sample C3 in comparison to sample C1 which causes in a decrease in the bandgap energy. The increment in band gap energy was due to a decrease in crystallite size and a comparable statement was also stated in the literature [21]. As the crystallite size approaches to the nanoscale, the number of atoms or molecules in the crystal will decrease that will lead to the reduction in orbital overlapping of corresponding energy level. This causes the creation of narrow valence and conduction bands which results in increase in optical band gap between the conduction and valance band. Due to the quantum size effect, the movement of the electron is constrained and restricted as the band gap energy increases [21]. The sample containing the higher $Ca(NO)_3$ molarity shows a higher peak intensity compared to other samples. The band gap can be estimated by the plot of $(\alpha h\nu)^2$ with photon energy ($h\nu$) as shown in Figure 7. The band gap of Samples C1, C2, and C3 were 5.50 eV, 5.55, and 5.68 eV of the nitrate concentration of 0.4, 1, and 1.6 M, respectively.

Conclusion

In the current study, we have synthesized the $Ca(OH)_2$ nanomaterials by the chemical precipitation route. The molarity of nitrate was changed at different concentrations of nitrates i. e. 0.4 M, 1 M, and 1.6 M. all the prepared samples were then characterized by XRD, FESEM, and UV-Vis spectroscopy techniques. The result obtained from the current

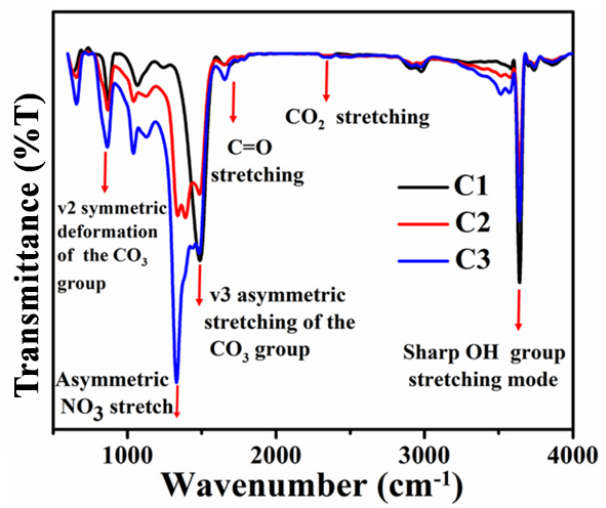

Figure 5: FTIR spectrum of sample C1, C2, and C3.

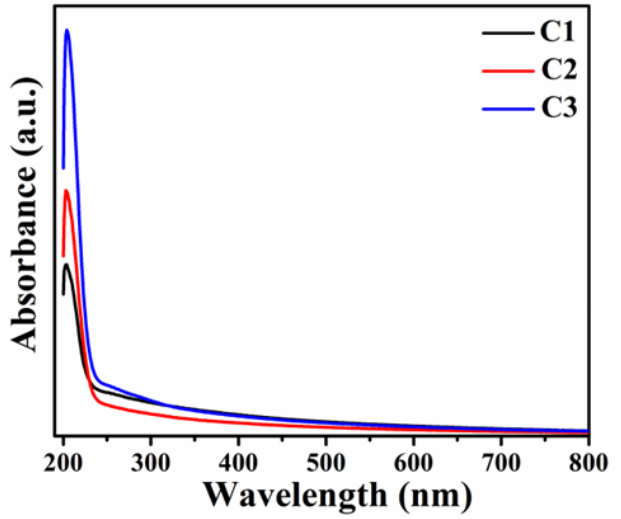

Figure 6: Absorption spectra of sample C1, C2, and C3.

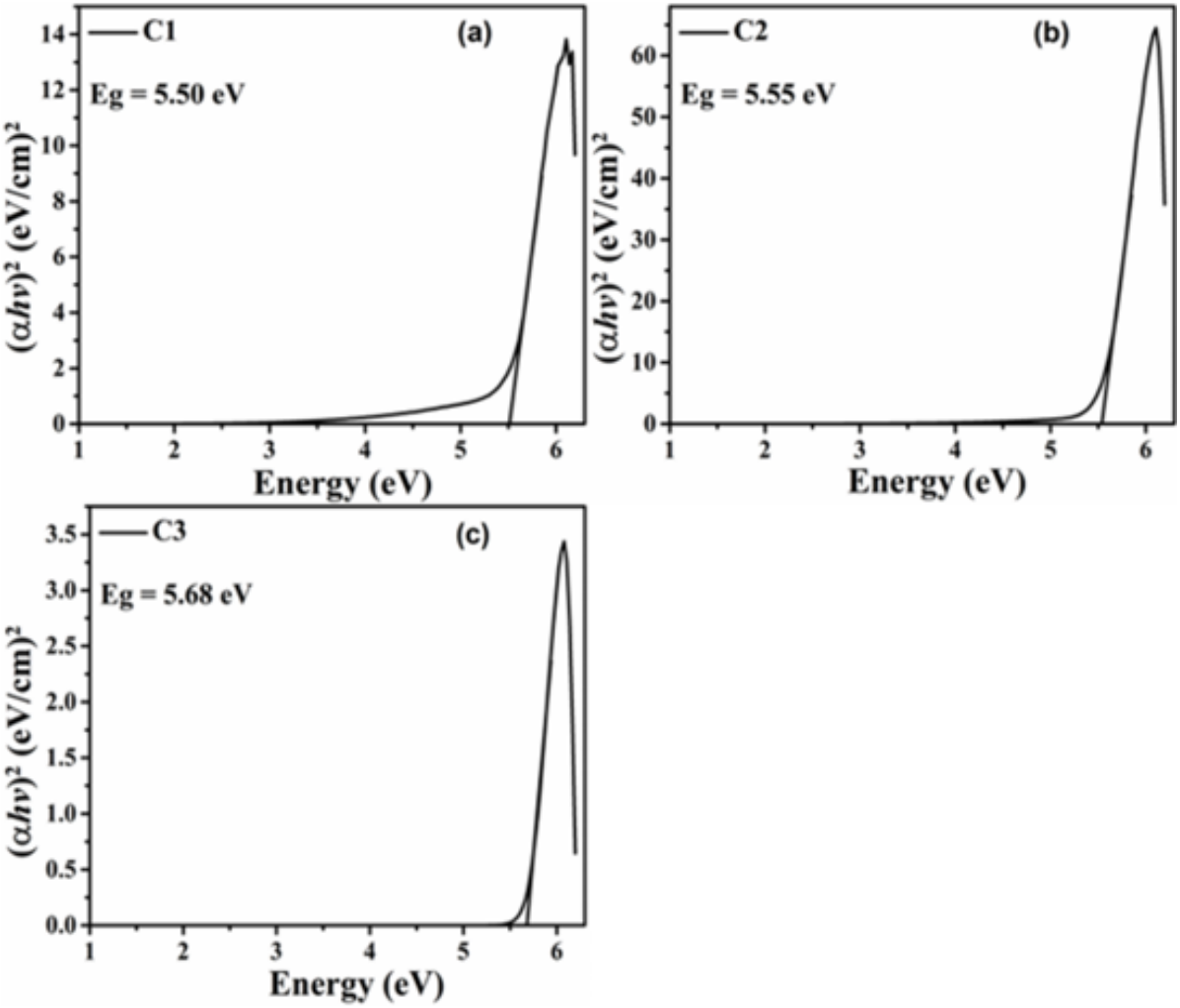

Figure 7: Tauc's plot of sample (a) C1, (b) C2, and (c) C3.

study proves that by changing the molarity of solution it is possible to control the size of NPs from about 103 nm to 64 nm. The decrease in the crystallite size results increase in optical band gap from 5.50 to 5.68 eV. The optical properties match with the XRD results of all samples and also was in accordance with the literature.

Acknowledgements

The author PK acknowledges the sophisticated analytical instrument facility (SAIF) for the XRD measurements and FESEM studies as well as Central Analytical Facility (CAF) for the other characterization at Manipal University Jaipur. The author Akash thanks to the CSIR (Sanction No. 09/1264(0005)/2020-EMR-I) for providing financial assistance in the form of a scholarship.

References

1. Schaube F, Koch L, Wörner A, Steinhagen HM. 2012. A thermodynamic and kinetic study of the de- and rehydration of $Ca(OH)_2$ at high H_2O partial pressures for thermo-chemical heat storage. Thermochim Acta 538: 9-20. https://doi.org/10.1016/j.tca.2012.03.003
2. Schmidt M, Gutierrez A, Linder M. 2017. Thermochemical energy storage with $CaO/Ca(OH)_2$ – Experimental investigation of the thermal capability at low vapor pressures in a lab scale reactor. *Appl Energy* 188: 672-681. https://doi.org/10.1016/j.apenergy.2016.11.023
3. Feng PH, Zhao BC, Wang RZ. 2020. Thermophysical heat storage for cooling, heating, and power generation: a review. *Appl Therm Eng* 166: 114728. https://doi.org/10.1016/j.applthermaleng.2019.114728
4. Gollscha M, Afflerbachb S, Angadia BV, Linder M. 2020. Investigation of calcium hydroxide powder for thermochemical storage modified with nanostructured flow agents. *Solar Energy* 201: 810-818. https://doi.org/10.1016/j.solener.2020.03.033
5. Castano SV, Plante LA, Shimoda EC, Wang S, Neithalath B, et al. 2021. Calcination-free production of calcium hydroxide at sub-boiling temperatures. *RSC Adv* 11: 1762-1772. https://doi.org/10.1039/D0RA08449B
6. Dolle K, Bajeami B. 2016. Calcium hydroxide as an alternative alkali for the oxygen bleaching stage of kraft pulp. *Cellulose Chem Technol* 50(9-10): 1055-1060.
7. Mohammadi Z, Dummer PMH. 2011. Properties and applications of calcium hydroxide in endodontics and dental traumatology. *Int Endod J* 44(8): 697-730. https://doi.org/10.1111/j.1365-2591.2011.01886.x
8. Zhang S. 2014. A new nano-sized calcium hydroxide photocatalytic material for the photodegradation of organic dyes. *RSC Adv* 4: 15835-15840. https://doi.org/10.1039/C4RA00081A
9. Rehmaan K, Saunders WP, Eoye RH, Shark SW. 1996. Calcium ion diffusion from calcium hydroxide-containing materials in endodontically-treated teeth: an in vitro study. *Int Endod J* 29(4): 271-279. https://doi.org/10.1111/j.1365-2591.1996.tb01381.x

10. Watcharathamrongkul K, Jongsomjit B, Phisalaphong M. 2010. Calcium oxide based catalysts for ethanolysis of soybean oil. *Songklanakarin J Sci Technol* 32(6): 627-634.

11. Akash, Harish, Kumari J, Mukhopadhyay AK, Kumar P. 2022. Effect of nitrate doping on the properties of chemically synthesized calcium hydroxide nanoparticles. *Chemistry Select* 7(24): e202200417. https://doi.org/10.1002/slct.202200417

12. Kumar TV, Chary AS, Bhardwaj S, Awasthi AM, Reddy SN. 2013. Dielectric relaxation, ionic conduction and Complex impedance studies on $NaNO_3$ fast ion conductor. *International Journal of Materials Science and Applications* 2(6): 173-178. https://doi.org/10.11648/j.ijmsa.20130206.12

13. Kumari J, Harish, Akash, Pandey A, Kumar P, et al. 2022. Synthesis and characterization of nanostructure calcite thin films deposited by dip coating. *Mater Today Proc* 60(Part 1): 306-310. https://doi.org/10.1016/j.matpr.2022.01.225

14. Kumar D, Singh M, Singh AK. 2018. Crystallite size effect on lattice strain and crystal structure of Ba1/4Sr3/4MnO3 layered perovskite manganite. *AIP Conference Proceedings* 1953(1): 030185. https://doi.org/10.1063/1.5032520

15. Sulungbudi GT, Yuliani, Lubis WZ, Sugiarti, S., Mujamilah.: Controlled growth of iron oxide magnetic nanoparticles via co-precipitation method and $NaNO_3$ addition. *Jurnal Sains Materi Indonesia* 18(3): 136-143. https://doi.org/10.17146/jsmi.2017.18.3.4122

16. Harish, Kumar P, Akash, Kumari J, Kumar L, et al. 2022. Influence of chemical synthesis process on the properties of calcium hydroxide nanoparticles. *Mater Today Proc* 60(Part 1): 153-159. https://doi.org/10.1016/j.matpr.2021.12.282

17. Samanta PK, Bandyopadhyay AK. 2012. Chemical growth of hexagonal zinc oxide nanorods and their optical properties. *Appl Nanosci* 2: 111-117. https://doi.org/10.1007/s13204-011-0038-8

18. Samanta PK. 2020. Band gap engineering, quantum confinement, defect mediated broadband visible photoluminescence and associated quantum States of size tuned zinc oxide nanostructures. *Optik* 221: 165337. https://doi.org/10.1016/j.ijleo.2020.165337

19. Samanta A, Chanda DK, Das PS, Ghosh J, Mukhopadhyay AK, et al. 2016. Synthesis of nano calcium hydroxide in aqueous medium. *J Am Ceram Soc* 99(3): 787-795. https://doi.org/10.1111/jace.14023

20. Harish, Kumar P, Kumari S, Debnath M, Salim A, et al. 2022 Tuning the antimicrobial efficacy of nano-$Ca(OH)_2$ against *E. coli* using molarity. *J Mater Sci* 57(17): 1-21. https://doi.org/10.1007/s10853-022-07198-5

21. Wang R, Lang J, Liu Y, Lin Z, Yan X. 2015. Ultra-small, size-controlled $Ni(OH)_2$ nanoparticles: elucidating the relationship between particle size and electrochemical performance for advanced energy storage devices. *NPG Asia Mater* 7: e183. https://doi.org/10.1038/am.2015.42